High Resolution Wide Swath SAR Imaging - System Performance and Influence of Perturbations

Nicolas Gebert, Gerhard Krieger, Alberto Moreira
Microwaves and Radar Institute, DLR, 82234 Oberpfaffenhofen, Germany
nico.gebert@dlr.de

***Abstract*—The displaced phase centre (DPC) technique enables a wide swath SAR with high azimuth resolution. In classic DPC systems, pulse repetition frequency (PRF), sensor velocity and antenna length underlie a stringent timing requirement to ensure uniform sampling of the synthetic aperture. This constraint can be overcome by the use of a reconstruction algorithm, which enables a recovery of the unambiguous azimuth (Doppler) spectrum also in case of a non-uniform sampling. This paper illustrates the principle of the reconstruction and explains its limitations and the impacts on the ambiguity suppression. The potential of the algorithm when applied to DPC systems like TerraSAR-X with its split receive antenna is demonstrated and the benefits resulting from the additional receive aperture regarding swath width and resolution are pointed out. Further on, the impact of additive and phase noise on the reconstruction and its sensitivity against these perturbations are shown.**

I. INTRODUCTION

A. Multi-Aperture Sampling

Several innovative techniques using multiple receiver apertures have been suggested to overcome the inherent limitations of SAR to perform High-Resolution Wide-Swath imaging [1]-[6]. For optimum performance, the along-track offsets of the n sub-apertures have to result in equally spaced effective phase centres thus leading to a uniform sampling of the received signal. In a classical Displaced Phase Centre Antenna (DPCA) system (cf. Fig. 1, left), the platform velocity v and the sub-aperture distance $\Delta x = x_{i+1} - x_i$ are fixed, which requires a specific PRF to fulfill the timing constraint for uniform sampling:

$$PRF = \frac{2 \cdot v}{n \cdot \Delta x} \tag{1}$$

However, such a rigid selection of the PRF may be in conflict with the timing diagram for certain incident angles. It will furthermore exclude the opportunity to use an increased PRF for improved azimuth ambiguity suppression.

B. Reconstruction from Non-Uniform PRF

As presented in more detail in [6] and [7], the ambiguous Doppler spectrum of a non-uniformly sampled SAR signal can be recovered unambiguously by applying a system of reconstruction filters. The algorithm is based on regarding the data acquisition in a multi-aperture SAR as a linear system with multiple receiver channels, each described by a linear filter $h_i(t)$ with transfer function $H_i(f)$ (cf. Fig. 1, middle). According to a generalization of the sampling theorem, a band-limited signal $u(t)$ is uniquely determined in terms of the samples of the responses $h_i(t)$ of n linear systems with input $u(t)$ sampled at $1/n$ of the Nyquist frequency [8]. Then, the reconstruction consists essentially of n linear filters $P_i(f)$ which are individually applied to the subsampled signals of the receiver channels and then combined coherently (cf. Fig. 1, middle). The reconstruction filters can be derived from the inversion of a matrix $\mathbf{H(f)}$ consisting of the n transfer functions $H_i(f)$. Then, $\mathbf{H(f)}^{-1}$ yields in its columns the filters P_i, given as a composition of n bandpass filters (cf. Fig. 1, right). This corresponds to solving a linear system of equations made up by the functions $H_i(f)$ and $P_i(f)$.

II. DISCRETE-TIME PROCESSING

In this section, an illustrative approach to explain the principle and limitations of the reconstruction algorithm is given.

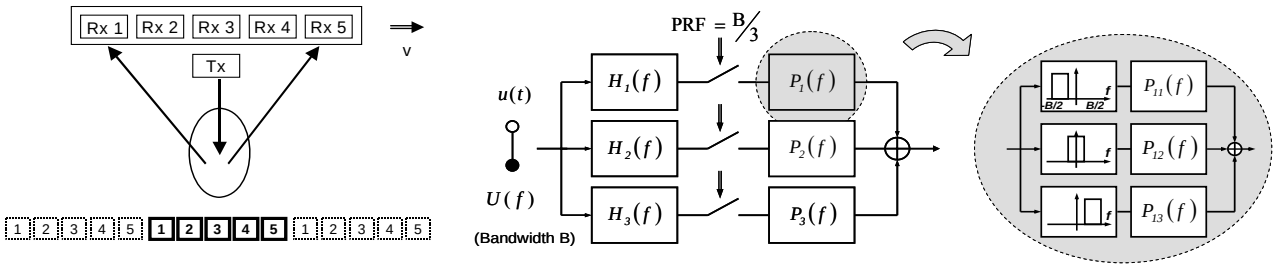

Figure 1. **Left**: DPCA system. The effective phase centres of the actual transmitter (Tx) and receiver (Rx) positions are shown as solid squares. Dotted squares stand for previous and subsequent transmit pulses. **Middle**: Reconstruction for multi-channel subsampling in case of three channels. **Right**: Each reconstruction filter P_i consists of n bandpass filters P_{ij}.

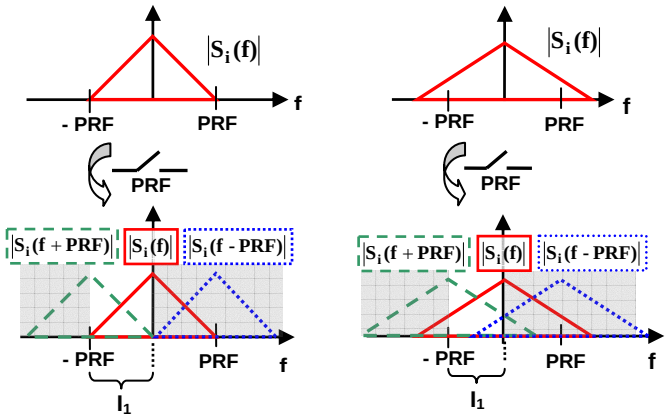

Figure 2. **Left**: Spectrum of signal limited to *[-PRF, PRF]* at receiver *i* before (top) and after (bottom) sampling with *PRF*. **Right**: Spectrum of signal at receiver *i* before (top) and after (bottom) sampling with *PRF*.

At first, consider a system with *n=2* apertures and *U(f)* limited to *[-PRF, PRF]*. Then, Fig. 2 on the left shows the spectrum of the band-limited signal $S_i(f)=H_i(f)\cdot U(f)$ 'seen' at the receiver *i* before (top) and after (bottom) sampling. As can be observed, for any frequency, the subsampled signal comprises not more than two (in general: *n*) frequency components, as not more than one spectrum (in general: *n-1* spectra) of the periodic continuation overlaps with the original spectrum. Hence, the spectra $S_1(f)$ and $S_2(f)$ can be weighted and combined in such a way, that the component of the original spectrum is recovered, while the shifted component is cancelled. With P_{ij} denoting the reconstruction filter for receiver *i* on the frequency interval *j*, this requires the following equations to hold true on the interval I_1 (cf. Fig. 2, bottom, left):

$$\begin{aligned} P_{11}(f)\cdot H_1(f)\cdot U(f)+P_{21}(f)\cdot H_2(f)\cdot U(f) &\overset{!}{=} U(f) \\ P_{11}(f)\cdot H_1(f+prf)\cdot U(f)+P_{21}(f)\cdot H_2(f+prf)\cdot U(f) &\overset{!}{=} 0 \end{aligned} \qquad (2)$$

By setting up the equations on the other intervals and shifting them to I_1, one obtains the linear system introduced in section I:

$$\mathbf{H(f)}\cdot\mathbf{P(f)}=1 \Leftrightarrow \mathbf{P(f)}=\mathbf{H(f)}^{-1} \qquad (3)$$

Let us now consider a scenario where the bandwidth of the signal exceeds *n·PRF*. For *n=2*, an example for the spectrum of such a signal is given in Fig. 2 on the right, before (top) and after (bottom) sampling. In contrast to the band-limited case, it is observed that for each frequency the sampled signal consists of up to three contributions, as the spectra of the periodic continuation may overlap. For the general case, this means that more than *n* spectra coincide at a certain frequency. From the mathematical point of view, this results in a linear system of equations that is under-determined and consequently the original spectrum can in general not be reconstructed exactly. As it was shown in the theoretical approach presented in [9], a complete suppression of the contributions from the shifted spectra is not achieved. This is due to the fact, that the filters P_i are determined as if the signal bandwidth was limited to $\pm n\cdot PRF/2$. Hence only the ambiguous energy within the band $[-n\cdot PRF/2, n\cdot PRF/2]$ of the original signal is cancelled by the reconstruction. All energy outside this band is not well suppressed and finally gives rise to ambiguities in the reconstructed signal. This may be reduced by selecting appropriate sub-bands and/or azimuth weighting during the reconstruction.

III. Simulation Results

First simulations applying the suggested algorithm were carried out for the reconstruction of real SAR-data, a multistatic satellite configuration and the dual receive antenna of TerraSAR-X [6] [7]. Here, we will present simulation results comparing the ambiguity suppression of a TerraSAR-X scenario with full receive antenna (cf. Table I, bottom left) and split receive antenna, the Dual Receive Antenna mode (DRA) (cf. Table I, top left). The relevant system parameters are summarized in Table I. The antenna pattern was approximated by a *sin(x)/x* characteristic.

TABLE I. : Parameters for DRA Mode and Monostatic System.

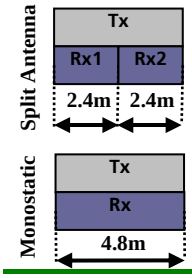

Wavelength	3.1 cm	
PRF on transmit	variable	
Velocity	7600 m/s	
Antenna Length (Tx)	4.8 m	
Number of Subapertures (Rx)	1	2
Sub-Aperture Length (Rx)	4.8 m	2.4 m
Slant Range	~ 700 km	
Orbit Height	~ 510 km	

In the following, ambiguity suppression is measured as the ratio of the peak powers from the mainlobe to the 1st order ambiguity at Doppler frequency $\pm PRF$ of the focused point target response. This ratio is referred to as '1st order ambiguity suppression' and it is determined for a transmit *PRF* varying from 1.5 kHz to 3.5 kHz in an approach that considers only the azimuth dimension. 2-dimensional simulations were also carried out and showed in general the same behavior.

In a first step, focusing is done by a matched filter with a constant Doppler bandwidth $B_{D,P}$ of 2.3 kHz for each of the systems. This is the nominal bandwidth used for TerraSAR-X, resulting in a resolution (3 dB width of power) of 3.2 m for the DRA and 3.4 m for the monostatic configuration. Fig. 3 on the left shows the resulting ambiguity suppression for these systems. Note that for the monostatic case only a *PRF* higher than $B_{D,P}$ makes sense while the DRA allows for a minimum *PRF* of half of $B_{D,P}$.

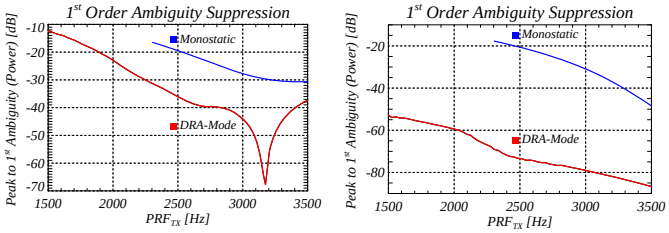

Figure 3. Ambiguity suppression of DRA (red) and monostatic mode (blue) for *sin(x)/x* pattern (**left**) and ideal tapering (**right**).

The best suppression is achieved around a *PRF* of 3.17 kHz, what corresponds to uniform sample spacing, leading to a nearly complete cancellation of the ambiguous targets at ±*PRF*. The clear increase of the ambiguous power when the sampling gets more non-uniform is due to aliasing effects mentioned in section II. This becomes clear, when the ambiguity suppression is considered for a signal whose bandwidth is restricted to *1.9·PRF* by assuming an ideal antenna pattern. The result shows an almost complete suppression of the ambiguity (cf. Fig. 3, right). We observe that the 1st order ambiguity after reconstruction is strongly influenced by spectral energy at frequencies that correspond to 2nd and higher order ambiguities. As mentioned in section II this is due to the fact that only the ambiguous signal within the interval *[-n·PRF/2, n·PRF/2]* is cancelled by the reconstruction, but all spectral energy from higher frequencies adds to the ambiguity.

In a next step, we try to find an optimum combination of parameters to maximize the benefits for resolution and swath width. Therefore, a function $G(B_{D,P},PRF)$ is defined as the product of the inter-pulse period PRF^{-1}, thus determining directly the unambiguous swath width, and the inverse azimuth resolution δ_{Az}^{-1} normalized by the sensor velocity v. This function can be considered as expressing the information content of the imaged area in dependency of the chosen combination of *PRF* and $B_{D,P}$. The normalization of δ_{Az}^{-1} causes G to be the quotient of the effective bandwidth 'contributing' to the resolution, denoted B_{eff}, and the *PRF*.

$$G = v \cdot \delta_{Az}^{-1} \cdot PRF^{-1} = \frac{B_{eff}}{PRF} \qquad (4)$$

When analyzing G, we find its optimum situated along the straight line $B_{D,P}=2\cdot PRF$ for the DRA mode and along $B_{D,P}=PRF$ for the monostatic configuration. Hence, these ratios are chosen and the ambiguity suppression and the corresponding curves for G as a function of *PRF* are determined. The resulting characteristics for both configurations are shown in Fig. 4.

Assume a necessary suppression of the 1st order ambiguity of -25 dB. For the DRA, this requires a *PRF* of 2065 Hz while for the monostatic case 3085 Hz are necessary as can be seen from Fig. 4, top. Hence the inter-pulse periods defining the unambiguous swath width increased from 0.32 ms (monostatic) to 0.48 ms

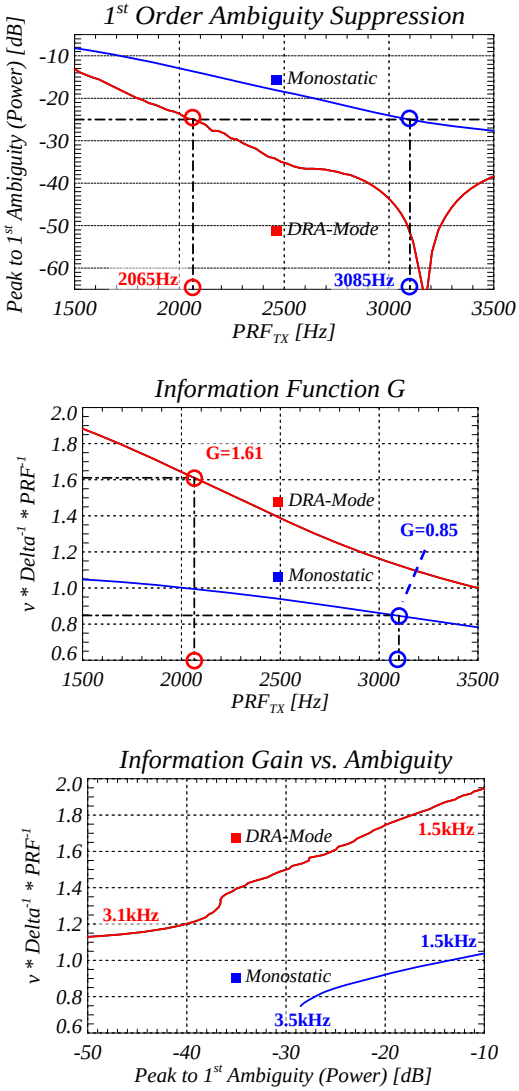

Figure 4. **Top**: 1st order ambiguity vs. *PRF* for DRA (red) and monostatic system (blue). **Middle**: Information Gain in dependency of *PRF* for DRA and monostatic configuration. **Bottom**: Information Gain over ambiguity suppression parameterized with *PRF*.

(DRA), resulting in a possible swath enlargement by a factor of 1.5

Regarding the respective values of G we obtain 1.61 (DRA) and 0.85 (monostatic) as marked in the middle plot. Determining the corresponding resolutions from G with the given *PRFs*, 2.3 m are achieved for the DRA while the monostatic case yields 2.9 m. Thus the resolution improved by a factor of 1.26. Multiplication of the two factors results in an overall gain of 1.89, which is near to the number of used sub-apertures. This overall gain corresponds to the ratio of the values of the respective gain functions labeled in the middle plot. Finally, Fig. 4, bottom, merges the above curves. This yields the characteristic of the information function G in dependency of the suppression ratio parameterized with *PRF* for the marked range. This allows to directly deter-

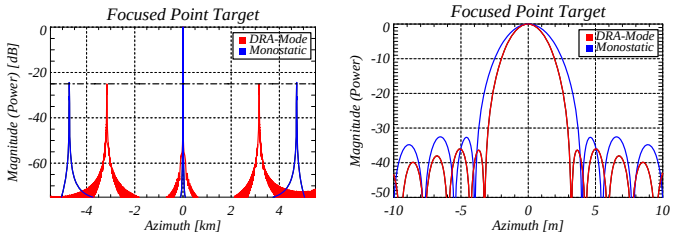

Figure 5. **Left**: Ambiguity at -25dB for focused point target responses of DRA (red, *PRF* ~2kHz) and Monostatic system (blue, *PRF* ~3kHz). **Right**: Mainlobes of point target responses showing the resolutions for DRA (red) and classical system (blue).

mine the achieved gain values of the two systems for a given suppression ratio.

For the values chosen above, the focused point target responses are given in Fig. 5. It demonstrates the constant ambiguity suppression for the different systems and their respective *PRFs* (left) and the improved resolution of the DRA with respect to the monostatic system (right).

The use of the split antenna in combination with the reconstruction algorithm allows for a reduced *PRF* and an improved azimuth resolution. This permits to increase the unambiguous swath width and to resolve timing conflicts in TerraSAR-X. The drawback of multi-aperture techniques is an increased amount of data to be handled. Furthermore, the noise level might rise as will be explained in the next section.

IV. Sensitivity against Noise

According to the theory of the generalized sampling theorem, the reconstruction in an ideal system is independent from the configuration as long as there are no identical samples. In a real scenario, where perturbations are taken into account, the configuration which determines the effective sample positions plays an important role.

A. Additive Noise

Consider independent additive noise in each of the receiver channels. In this case, the reconstruction always yields the signal *u(t)* and an additive output noise. Hence, the reconstruction and ambiguity suppression is not affected and the signal power at the output remains constant. In contrast, the noise power is a weighted sum of the input noises' spectral power densities that are scaled by the reconstruction filter functions $P_i(f)$ and the respective $SNR_{in,\,i}$ of this channel. For the simple case of white noise this yields a Signal-to-Noise-Ratio after the reconstruction (SNR_{out}) as follows:

$$SNR_{out} = \left(\sum_{i=1}^{n} \frac{E\left[|P_i|^2\right]}{n \cdot SNR_{in,i}} \right)^{-1} \qquad (5)$$

For the case of a system with two sub-apertures, one can say that the amplification of the SNR_{out} becomes stronger the more the actual sampling deviates from the case of uniform sampling. An example is given in the subsequent Fig. 6. On the left, it shows the dependency of the SNR_{out} on the distance between the phase-centers measured in percent of ideal uniform distance. 100% of uniform distance corresponds to a uniform sampling while 0% represents identical phase centre positions. The plot on the right presents the scaling in dependency of the *PRF* for a TerraSAR-X scenario with a sensor velocity of 7600 m/s and a distance of 2.4 m between the sub-apertures. The values in both plots are normalized to the optimum SNR_{out} achieved for uniform sampling. For TerraSAR-X that corresponds to a *PRF* of ~3.17 kHz, indicated by the red dashed vertical line. As can be observed, for the DPCA case considered, the noise floor rises by a factor of about 1.35. The respective *PRF* of ~2 kHz is marked by the black dashed line. Although degrading the system performance, this does not become a critical issue.

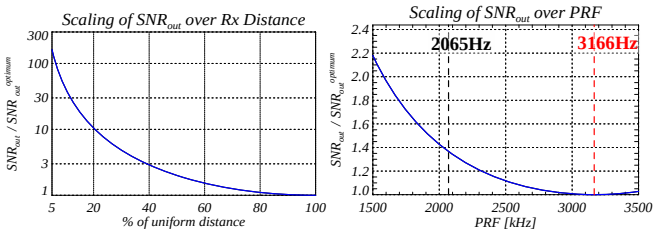

Figure 6. Scaling of noise floor normalized to the optimum achieved for uniform sample distance. **Left**: SNR_{out} in dependency of the receiver offset expressed in % of optimum distance. **Right**: SNR_{out} as a function of *PRF*.

Consider now a system with $n=3$ apertures and a $SNR_{in,i}$ of 10dB at each receiver. The resulting SNR_{out} is shown as a contour-plot in dependency of the offsets of Rx_2 and Rx_3 relative to Rx_1 (cf. Fig. 7, left). The curve is normalized to the minimum SNR_{out} achieved for uniform phase-centre configuration. As can be observed, for a given offset between 2 receivers, the optimum location for the 3rd receiver is not on its position for uniform sampling but it changes with the other phase centers' locations. The singularity marked as a dashed line corresponds to the case, where the positions of Rx_2 and Rx_3 lead to identical phase centres. The loci of the extreme values are presented on the right, where the upper curve corresponds to the minimum and the middle

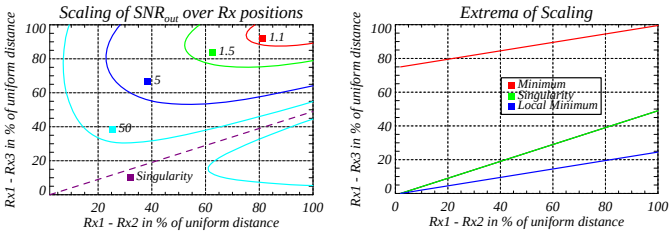

Figure 7. **Left**: Contour lines for scaling of noise floor normalized to the optimum achieved for uniform sample distance. **Right**: Loci of minimum (red), singularity (green) and local minimum (blue) of SNR_{out}. **Both** plots are shown in dependency of the offsets of Rx_2 (x-axis) and Rx_3 (y-axis) relative to Rx_1 expressed as a percentage of uniform distance.

one to the singularity while the lower curve represents a local minimum.

B. Phase Noise

Moreover, the impacts of phase noise on the reconstruction were examined. For this, a random Gaussian phase was added to the input signal of the reconstruction filters to simulate receiver phase noise. This was done for standard deviations of the phase from 5° to 35° and over a *PRF* from 1.5 kHz to 3.5 kHz leading to a maximum non-uniform sampling of approximately 40% of uniform sampling. On top of Fig. 8, the signal bandwidth was limited to *1.9·PRF* by an ideal pattern to avoid aliasing effects so that the impact of the phase noise itself can be observed. As one can see, the ambiguity suppression gets worse the higher the standard deviation of the phase noise is (cf. Fig. 8, left). The differences to the noise-free scenario that give the degradation caused by the phase noise are shown on the right. In a next step, the signals were not confined any more in bandwidth as simulations were carried out for the standard *sin(x)/x* pattern. In this case, one can see that the degradation of the ambiguity suppression is dominated by aliasing as only regions with high suppression are noticeably affected by the phase noise (cf. Fig. 8, bottom).

Further investigations have indicated that the resolution degrades only for very strong non-uniform sampling. In the considered range of *PRFs*, no degradation of the resolution was observed.

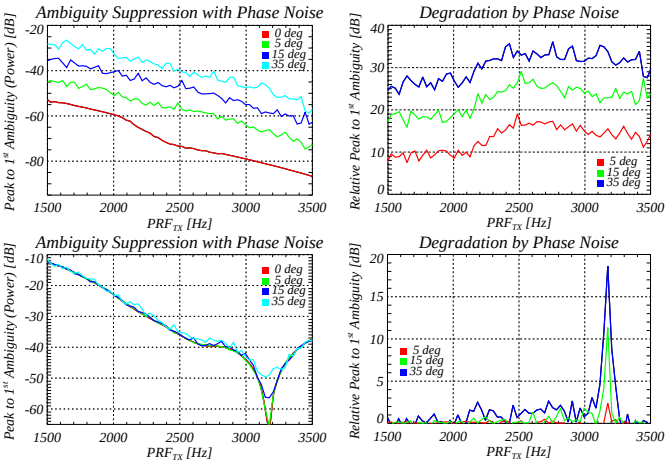

Figure 8. **Top left**: Peak-to-1st order ambiguity ratio as a function of *PRF* for different levels of phase noise and a signal band-limited to *1.9·PRF*. **Top right**: Degradation of the Peak-to-1st order ambiguity ratio for different levels of phase noise relative to the case without noise. **Bottom**: Peak-to-1st order ambiguity ratio (**left**) and degradation (**right**) for unlimited signal bandwidth.

V. SUMMARY

A reconstruction algorithm for the suppression of azimuth ambiguities in non-uniformly sampled data has been presented. The limitations inherent to the discrete-time processing and its consequences on the reconstruction were pointed out and demonstrated by simulation results. The algorithm is directly applicable to DPCA systems, like the HRWS SAR [2] or the dual receive antenna approaches in TerraSAR-X [5] and Radarsat-2 [4]. Its capability of ambiguity suppression allowing for improved resolution and an enlarged swath has been successfully demonstrated for the experimental DRA mode. In this context, the relation between ambiguity suppression and the benefits compared to the monostatic approach regarding swath width and resolution were presented. It should be noted that future systems optimized to multi-aperture applications will be clearly better able to exploit the potential of the reconstruction algorithm. For example, such a system might allow for pattern tapering minimizing higher order ambiguous energies disturbing the reconstruction. Moreover, the influence of perturbations on the reconstruction was investigated. For the case of additive noise an expression was given, how the noise floor rises in dependency of the sample positions. The stronger the sample positions deviate from uniform sampling, the more the *SNR* after the reconstruction degrades. For the examined DPCA system this scaling of noise is not critical. Furthermore, it was shown that phase noise has only in regions of high suppression a remarkable effect while being negligible when aliasing takes place.

REFERENCES

[1] A. Currie and M.A. Brown, "Wide-Swath SAR", IEE Proceedings - Radar Sonar and Navigation 139 (2), pp 122-135, 1992

[2] M. Suess, B. Grafmüller, R. Zahn, "A Novel High Resolution, Wide Swath SAR System", IGARSS 2001

[3] M. Younis, C. Fischer, W. Wiesbeck, „Digital Beamforming in SAR systems", IEEE Transactions on Geoscience and Remote Sensing 41 (7), pp. 1735-1739, 2003

[4] L. Brule, H. Baeggli, „Radarsat-2 Program Update", IGARSS 2002.

[5] J. Mittermayer, H. Runge, "Conceptual Studies for Exploiting the TerraSAR-X Dual Receiving Antenna", IGARSS 2003.

[6] G. Krieger, N. Gebert, A. Moreira, "Unambiguous SAR Signal Reconstruction from Non-Uniform Displaced Phase Centre Sampling", IEEE Geoscience and Remote Sensing Letters, Vol. 1, No. 4, Oct. 2004

[7] G. Krieger, N. Gebert, A. Moreira, „Unambiguous SAR Signal Reconstruction from Non-Uniform Displaced Phase Center Sampling", IGARSS 2004

[8] J.L. Brown, "Multi-Channel Sampling of Low-Pass Signals", IEEE Transactions on Circuits and Systems 28 (2) , pp.101-106, 1981

[9] N. Gebert, G. Krieger, A. Moreira, „SAR Signal Reconstruction from Non-Uniform Displaced Phase Center Sampling in the Presence of Perturbations", IGARSS 2005